Journal of Technomaterial Physics
Journal homepage: https://talenta.usu.ac.id/JoTP

Effect of Barium Hexaferrite Doped Yttrium (Y^{3+}) On The Microwave Absorption By Solid-State Reaction Methods

Muhammad Sontang Sihotang[1*], Marc Antonio Angelo[1], Marzuki Naibaho[2,3], Maulidita[1], Novita Ichsan[1], and Masno Ginting[3*]
[1]*Department of Physics, Universitas Sumatera Utara, Medan, 20155, Indonesia.*
[2]*Department of Physics, Universitas Indonesia, Depok 16424, Indonesia.*
[3]*Advanced Materials Research Center (PRMM), National Research and Innovation Agency (BRIN), Complex Puspiptek Building 440-441, Tangerang-South, Banten. 15314. Indonesia.*
[*]Corresponding Author: muhammad.sontang@usu.ac.id, masn001@brin.go.id

ARTICLE INFO
Article history:
Received 12 December 2024
Revised 20 April 2025
Accepted 21 April 2025
Available online 22 April 2025

E-ISSN: 2656-0755
P-ISSN: 2656-0747

How to cite:
M. S. Sihotang, M. A. Angelo, M. Naibaho, Maulidita, N. Ichsan, M. Ginting "Effect of Barium Hexaferrite Doped Yttrium (Y^{3+}) On The Microwave Absorption By Solid-State Reaction Methods," Journal of Technomaterial Physics, vol. 07, no. 01, pp. 63-70, Feb. 2025, doi: 10.32734/jotp.v7i1.19265.

ABSTRACT
Yttrium-substituted M-type barium hexaferrite was successfully synthesized using the solid-state reaction method. X-ray diffraction (XRD) confirms that all various samples have a single phase (for x = 0,0 and 0,1), have increased trend for crystal size (from 56,99 to 59,34 nm), cell volume (from 697,9161 to 701,2375 Å), and lattice parameter (a = 5,8948 to 5.9024 and c = 23,1918 to 23,2422) caused by ion substitution increased. SEM-EDX figure shows that the particle shape of yttrium doped barium hexaferrite is hexagonal, and there is a growth in particle size as the amount of doping increases from 1.050 to 1.202 µm and also the amount of Y^{3+} ion doping increases, the number of Fe atoms decreases and the number of Y atoms increases. The materials were characterized using a Vector Network Analyzer (VNA), which shows minimum reflection loss of x = 0.1 reaches -7,34 dB in the X-band for a thickness of 1.5 mm, better sample variation when compared to other sample variations.

Keywords: Yttrium-Substituted M-Type Barium Hexaferrite, Crystal Structure, Solid-State Reaction Method, Morphology, Reflection Loss.

ABSTRAK
Barium heksaferrit tipe-M yang disubstitusi Yttrium berhasil disintesis dengan metode *solid-state reaction*. *X-Ray Diffraction* (XRD) mengkonfirmasi bahwa semua sampel yang berbeda memiliki fasa tunggal (untuk x = 0,0 dan 0,1), memiliki tren peningkatan ukuran kristal (dari 56,99 menjadi 59,34 nm), volume sel (dari 697,9161 menjadi 701,2375 Å), dan parameter kisi (a = 5,8948 menjadi 5,9024 dan c = 23,1918 menjadi 23,2422) yang disebabkan oleh peningkatan substitusi ion. Hasil SEM-EDX menunjukkan bahwa bentuk partikel barium heksaferrit yang didoping yttrium berbentuk heksagonal dan terjadi pertumbuhan ukuran partikel seiring dengan bertambahnya jumlah doping dari 1,050 menjadi 1,202 µm dan juga bertambahnya jumlah doping ion Y^{3+}, jumlah atom Fe berkurang dan jumlah atom Y bertambah. Material dikarakterisasi dengan menggunakan *Vector Network Analyzer* (VNA), menunjukkan bahwa *reflection loss* minimum x = 0,1 mencapai - 7,34 dB pada pita-X untuk ketebalan 1,5 mm, merupakan variasi sampel yang lebih baik jika dibandingkan dengan variasi sampel lainnya.

Kata kunci: Barium Heksaferit Tipe-M disubstitusi Yttrium, Struktur Kristal, Metode *Solid-State Reaction*, Morfologi, *Reflection Loss*

1. Introduction

Nowadays, technological progress is growing rapidly and unstoppable. The evidence of technological advancement that we can feel is the speed of the internet network, radar systems, improved communication devices, and most importantly, the use of wireless electronic and telecommunications devices [1], [2]. Widespread use of wireless technologies and telecommunication devices at higher frequencies caused interference and electromagnetics (EM) pollution. The advancement of EM wave-absorbing materials is urgently needed to solve this problem [1]. Microwave absorption materials (MAMs) have attracted a lot of attention from technologists and scientists due to their application as electromagnetic (EM) shielding. Many researchers desired to fabricate absorbing properties with excellent characteristics, such as thinness, lightweight, wide bandwidth absorption, and strong absorption. MAM's complex permittivity and permeability are crucial to microwave absorption materials (MAM's) development [3], [4], [5].

Among numerous candidates, hexagonal ferrites as a magnetic material have high potential as an EM absorber. Hexagonal ferrites, prevalent referred to as hexaferrites, known as permanent magnetic [6], [7] has wide applications, such as high-frequency transformers [8], communication devices [9], memory storage applications [10], recording media [11], and microwave absorber [12]. The hexaferrites pervade into six series, namely U type ($Ba_4A_2Fe_{36}O_{60}$), Z type ($Ba_3A_2Fe_{24}O_{41}$), Y type ($Ba_2A_2Fe_{12}O_{22}$), W type ($BaA_2Fe_{16}O_{27}$), X Type ($Ba_2A_2Fe_{28}O_{46}$) and M type ($BaFe_{12}O_{19}$), where "A" can be inserted with the elements of Sr, Co, Ni or Zn [13], [14].

Barium hexaferrite is a ceramic material with a hexagonal crystal structure that can be used at a much higher frequency than other types of ferrites [14], [15], [16]. Barium hexaferrite has hard magnetic properties such as splendiferous chemical stability, resistivity of corrosion, large magneto anisotropy, high Curie temperature, high saturation magnetization, and high coercivity. It is also cheap to produce [17], [18], [19], [20], [21]. Some studies have synthesized $BaFe_{12-x}Y_xO_{19}$ materials ($_x$ = 0,0; 0,3; 0,5; 0,7; and 0,9) hexaferrites by citrate precursor method. They found out that the total absorption effectiveness of electromagnetic interference (EMI) is -80.07 dB in the X-band range, notably at a yttrium variation x = 0.7, reveal able to absorb as far as -98.08 dB at a frequency range of 10 GHz. Barium hexaferrite-substituted yttrium exhibits the optimum ability to shield electromagnetic waves. The many techniques of synthesis to prepare M-type hexaferrite so far include co-precipitation [22], [23], spray pyrolysis [24], sol-gel method [25], sol-gel auto combustion [26], hydrothermal synthesis [27], glass crystallization [28], microemulsion [29], and solid-state reaction [30], [31] Solid-state reaction is a classic method of mixing materials in the form of solids without using a solvent medium. Solid-state reaction has a simple process, does not require many precursors, is economical, and is easy to perform on an industrial scale [32].

In this paper, we have prepared $BaFe_{12-x}Y_xO_{19}$ (x = 0,0; 0,1; 0,3) and synthesized it using the solid-state reaction method. Therefore, we investigated the effect of substituted ions on the structure, phase, morphology, permittivity, permeability, and reflection loss from $BaFe_{12-x}Y_xO_{19}$.

2. Materials and Methods

In order to prepare the sample, all analytical grades reagents chemicals such as Iron (III) Oxide (Fe_2O_3) (96%), Yttrium oxide (Y_2O_3) (99.99%) were purchased from Sigma Aldrich, and Barium Carbonate ($BaCO_3$) (99%) were purchased from Merck Germany.

The raw materials were weighed in stoichiometric proportion and then mixed and ground in an agate mortar for about one hour. Then, at the second stage, the ground powder was pressed into tablets using a round steel die of 30 mm diameter with a pressure of 4 tons and afterward pre-sintered in alumina crucibles for six h at 800 ^oC. The pre-sintered sample was reground in an agate mortar for about 0.5 h. Thereafter, the pre-sintered powder samples were sintered at 1200 ^oC for three hours. The fine sample subsequently was reground until it passed 200 mesh. Then, the sample will be characterized using X-ray diffraction (XRD - type SmartLab-Rigaku), Scanning Electron Microscope – Energy Dispersive X-Ray (SEM-EDX – type JEOL JSM-IT200), and Vector Network Analytical (VNA – type Advantest type R3770 300 kHz - 20 GHz).

3. Results and Discussion

3.1. X-Ray Diffraction (XRD) Analysis

XRD patterns in Fig.1 show the result of barium hexaferrite-substituted yttrium. The diffraction peaks were confirmed to the barium hexaferrite standard pattern of the ICDD Pattern No. 01-084-0757. There are eleven diffraction peaks identified: 22.95° (006), 30.27° (110), 32.14° (017), 34.05° (114), 37.02° (023),

40.25° (025), 42.35° (026), 54.97° (127), 56.50° (0211), 62.96° (220), 67.24° (2014), 72.49° (317).

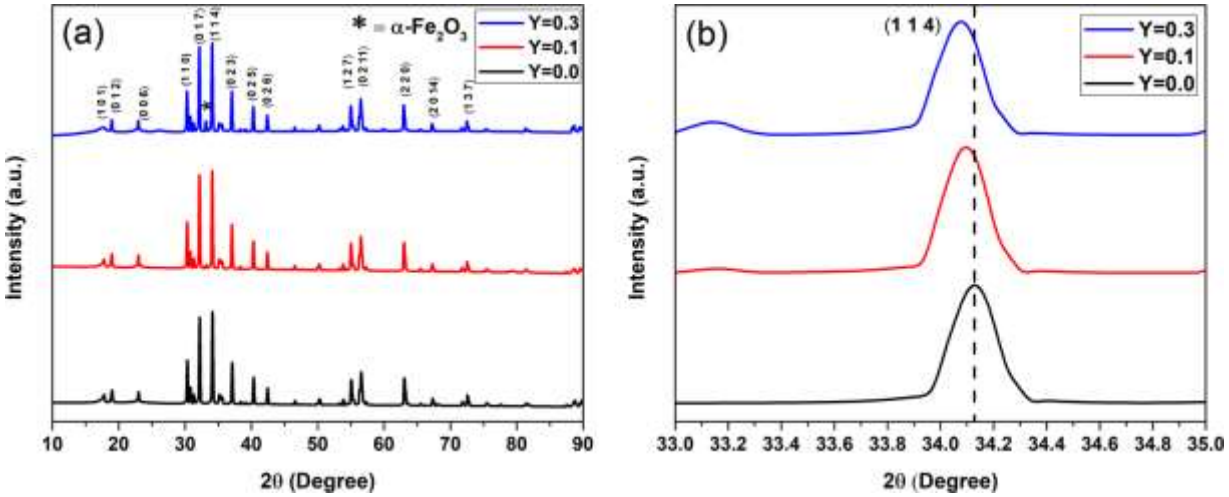

Figure 1. (a) XRD graph non and substituted samples of barium hexaferrite-substituted yttrium (b) magnified view of Bragg peak position (1 1 4) of barium hexaferrite-substituted yttrium.

Based on the figure, all samples display a well-defined single-phase hexagonal crystal structure. However, in the sample with x = 0.3, a small peak corresponding to α-Fe_2O_3 is detected between the (0 1 7) and (1 1 4) peaks, indicating some imperfections in crystallization. The prominent diffraction peak pattern can be categorized into various (hkl) indices of the same $BaFe_{12-x}Y_xO_{19}$ compound, which ideally exhibits the hexagonal structure characteristic of pure barium hexaferrite (as described by the P63/mmc space group). Figure 1(b) provides a closer look at the higher peaks in the diffractograms of barium hexaferrite-substituted yttrium, highlighting a shift in the XRD peak (1 1 4) as the yttrium content increases. Additionally, there is a reduction at peak (1 0 1) with higher doping levels of Barium Hexaferrite. This change is attributed to the larger ionic radius of Y^{3+} (0.9 Å) compared to Fe^{3+} (0.64 Å), which influences the crystal structure of barium hexaferrite.

Table 1. Peak analysis parameter of yttrium doped M-Type hexaferrite

Composition (x)	a (Å)	c (Å)	FWHM	c/a	Crystalline size (D) (nm)	V $(Å)^3$
0.0	5.8948	23.1918	0.1458	3.934	56.99	697.9161
0.1	5.8968	23.2122	0.1411	3.936	58.59	699.0041
0.3	5.9024	23.2422	0.1400	3.937	59.34	701.2375

The analysis of the peak parameters in Table 1 shows that the lattice constant experiences minimal variation, whereas the lattice constant *c* tends to trend substantially with higher levels of yttrium doping. Yttrium ion substitution caused the crystal size to increase with the increase of Y^{3+} doping (from 56.99 to 59.34 nm) due to the longwise length and crystal lengthwise. As a result, there is a growth expansion along the a- and c-axes. With yttrium doping, the mean average crystal size increases from 50.07 nm to 53.71 nm. Ratio parameter (c/a) is used to measure the structural type crystal of a sample; if the value of the lattice parameter ratio was less than 3.98, the materials were reflected to have an M-type hexagonal magnetoplumbite [33]. As the amount of yttrium increases, the narrowing of the observed X-ray scattering peak point increases crystal size. It can be seen in the Debye-Scherrer formula given in Equation (1)

$$D = \frac{k\lambda}{\beta \cos\theta} \quad (1)$$

Where D is crystalline size, λ is the wavelength of the x-ray, β is the value Full Width at Half Maximum (FWHM), k is the form factor of the crystal (0.9), θ is diffraction angle [34].

The alteration in the distance between planes results from substituting Y^{3+} ions for Fe^{3+} ions at the crystal cell. This substitution is challenging because Y^{3+} ions have a bigger ionic radii (0.9 Å) compared to Fe^{3+} ions

(0.64 Å). Consequently, there tends to be a higher concentration of Y^{3+} ions at the grain boundaries. Figure 1(a) illustrates how these Y^{3+} ions affect the intensity of the α-Fe_2O_3 phase as the yttrium concentration increases (specifically at x = 0.3). For effective substitution to occur, it is important that the valences and ionic radii of the two substances are compatible.

3.2. Microstructure Analysis

Image SEM of pure barium type-M and Yttrium-substituted hexaferrite materials with x = 0.0, 0.1, 0.3 are illustrated in Figure 2 (a-c). Micrographs show significant variations in grain size. The grain size distribution histogram is represented in Fig. 2 (d-e). The SEM micrographs reveal that the grain sizes for composition x = 0.0 range from 0.734 µm to 1.564 µm, with a median size of 1.050 µm. For composition x = 0.1, the grain sizes vary from a minimum of 0.734 µm to a maximum of 1.755 µm, resulting in an average particle size of 1.101 µm. In the case of composition x = 0.3, the grains have an average size of 1.202 µm, with sizes ranging from 0.885 µm to 1.77 µm. The hexagonal-shaped crystalline grains of ceramic magnet are observed in the SEM images. All samples exhibit well-defined shapes, boundaries, and homogeneity.

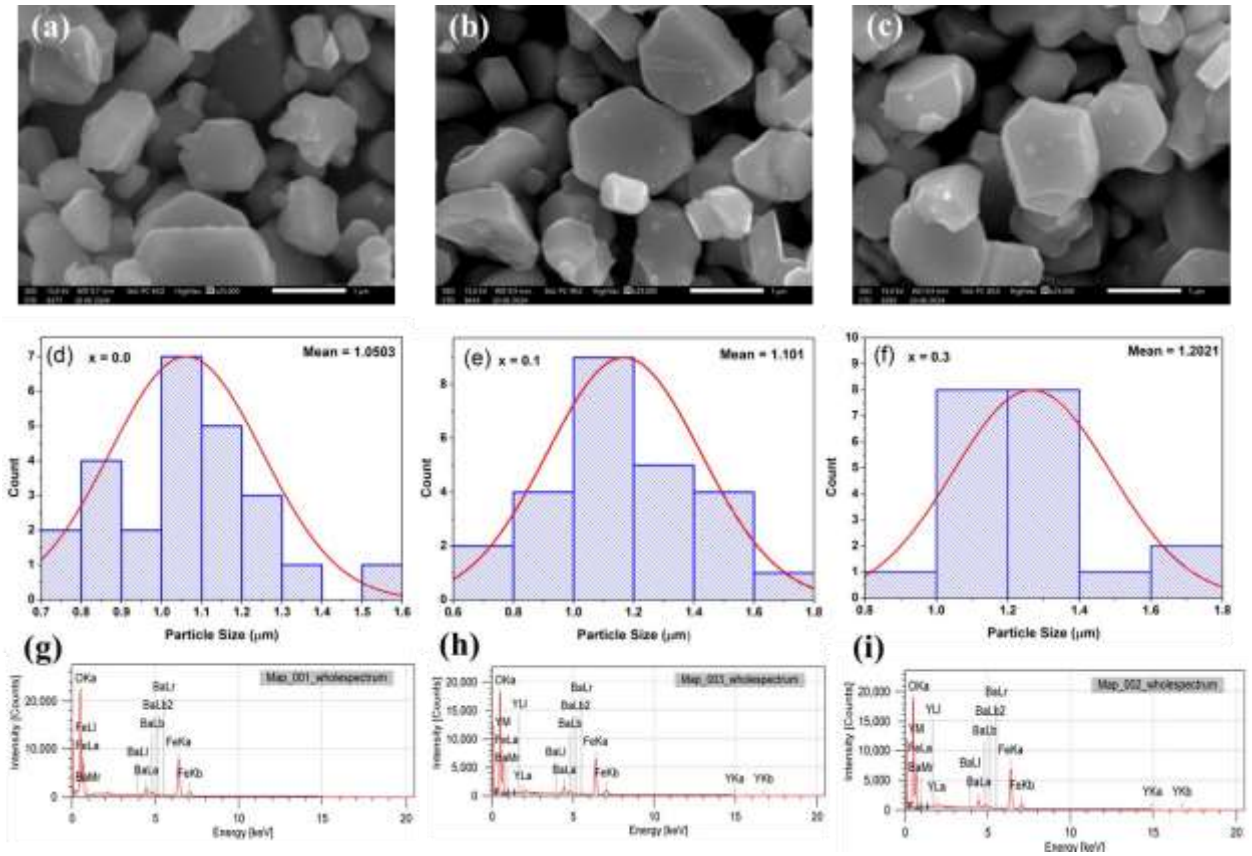

Figure 2. (a-c) SEM micrographs of barium hexaferrite-substituted yttrium (x = 0.0, 0.1, 0.3) (d-f) exposed grain size distribution of barium hexaferrite-substituted yttrium 0(x = 0.0, 0.1, 0.3) (g-i) EDX spectrum and mass % of yttrium substituted barium hexagonal ferrites.

When the material was sintered at 1200°C for 3 hours, oxygen was present. This oxygen availability results in the restriction of grain formation, with average grains being the small result. Even though it can be seen that there is a grain size increases when yttrium was substituted, according to the result of a decrease in oxygen vacancies, which can be seen in Table 2. The morphological study results confirm the material's M-type hexaferrite properties.

Figure 2 (g-i) yttrium was the simple one substituted element detected in all samples, which was inserted as the substituted element to proclaim the virginity of materials. Table 2 lists the percentage changes in elements in each sample. The proportion of yttrium detected through EDX rises with higher levels of Y doping. Concurrently, the amount of iron decreases as yttrium replaces it in a linear fashion. This observation reflects a strong alignment between the actual material and the theoretical design, thereby confirming the formation of M-type hexaferrite.

Table 2. The composition analysis of barium hexaferrite-substituted yttrium

x	Composition	Element (wt%)				
		Ba	Fe	Y	O	All
0.0	$BaFe_{12}O_{19}$	14.59	60.15	0.0	25.25	100
0.1	$BaFe_{11.9}Y_{0.1}O_{19}$	14.57	59.61	0.83	24.98	100
0.3	$BaFe_{11.7}Y_{0.3}O_{19}$	14.48	57.86	2.27	25.38	100

3.3. Microwave Absorption

Figure 3 shows a graph representing the reflection loss (RL) of BFYO ceramics (1.5 mm thickness) within 8-12 GHz. As Y^{3+} increases, the RL of BFYO ceramics experiences a very small shift for the minimum RL value. (from 11.32 to 11.7 GHz). For pure $BaFe_{12}O_{19}$, the -5 dB RL bandwidth (below -5dB, > 68.4% microwave absorption) of 11.24-11.78 GHz and a minimum reflection loss (RL) of -5.72 dB (73.99% microwave absorption) is obtained at 11.7 GHz. For $BaFe_{11.7}Y_{0.3}O_{19}$ the -5 dB RL bandwidth of 10.68-11.34 GHz and a minimum reflection loss (RL) of -6.26 dB (76.96% microwave absorption) is obtained at 11.32 GHz. The best absorption is obtained on $BaFe_{11.9}Y_{0.1}O_{19}$ ceramics with a minimum RL of -7.34 dB at 11.32 GHz and -5 dB RL bandwidth at 10.2 - 12 GHz. However, in $BaFe_{11.9}Y_{0.1}O_{19}$ ceramics, there are 2 RL valleys, namely -7.34 dB at 11.32 GHz (81.51% microwave absorption) and -6.46 dB (77.40% microwave absorption) at 11.72 GHz. $BaFe_{11.9}Y_{0.1}O_{19}$ ceramic shows the strongest microwave absorption capability at the X-band with 81.51% microwave absorption.

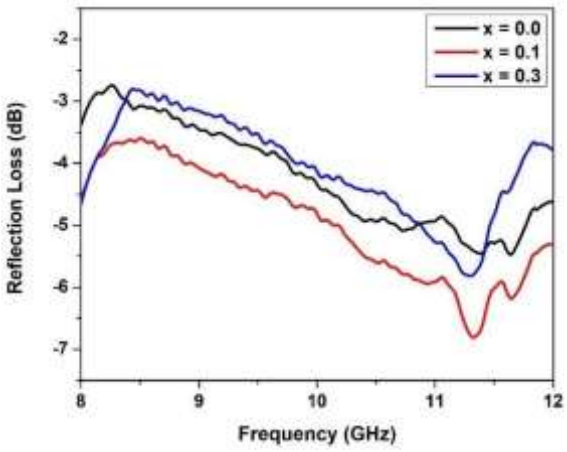

Figure 3. Reflection loss (RL) of barium hexaferrite-substituted yttrium

4. Conclusion.

The yttrium-doped barium hexaferrite $BaFe_{12-x}Y_xO_{19}$ was successfully synthesized by the solid-state reaction method using agate mortar. The single phase and hexagonal structure of the crystal were confirmed by XRD results. The XRD analysis results also exhibit an increase in crystalline size and lattice parameters as the amount of Y ions increases. The SEM image of yttrium doped M-type hexaferrite shows a hexagonal structure, and there is an increasing trend in average grain size with higher doped ion concentrations. Yttrium doped barium hexaferrite material exhibits the finest microwave absorption at yttrium ion variation x = 0.1, showing the highest reflection loss of -7.34 dB in the frequency range of 11.32 GHz with an absorption percentage of 81.51%. Barium hexaferrite-substituted yttrium was successfully synthesized by the solid-state reaction, showing the applicability of the material as an efficient microwave shielding method to reduce electromagnetic wave pollution, even with a simple synthesis method.

References

[1] E. Handoko, A. Subhan, S. Santosa, and M. I. Nugraha, "Microwave absorption performance of barium hexaferrite multi-nanolayers," in *Mater. Express*, vol. 10, no. 8, pp. 1328–1336, 2020. https://doi.org/10.1166/mex.2020.1811

[2] S. S. S. Afghahi, M. Jafarian, and Y. Atassi, "A promising lightweight multicomponent microwave absorber based on doped barium hexaferrite/calcium titanate/multiwalled carbon nanotubes," *J. Nanoparticle Res.*, vol. 18, no. 7, pp. 1–11, 2016, doi: 10.1007/s11051-016-3499-6.

[3] H. Pang, Y. Q. Bao, W. Z. Li, and Z. F. Ma, "Research advances in composition, structure and mechanisms of microwave absorbing materials," in Compos. Part B Eng., vol. 224, no. July, p. 109173, 2021. https://doi.org/10.1016/j.compositesb.2021.109173

[4] Y. Li, D. Li, H. Luo, F. Chen, X. Wang, and R. Gong, "Co-Evaluation of reflection loss and surface wave attenuation for magnetic absorbing material," *IEEE Trans. Antennas Propag.*, vol. 66, no. 11, pp. 6057–6060, 2018, doi: 10.1109/TAP.2018.2867070.

[5] M. F. Elmahaishi, R. S. Azis, I. Ismail, and F. D. Muhammad, "A review on electromagnetic microwave absorption properties: their materials and performance," *J. Mater. Res. Technol.*, vol. 20, pp. 2188–2220, 2022, doi: 10.1016/j.jmrt.2022.07.140.

[6] A. Serrano, E. García-Martín, C. Granados-Miralles, G. Gorni, J. López-Sánchez, S. Ruiz-Gómez, L. Pérez, A. Quesada, and J. F. Fernández, "Hexaferrite-based permanent magnets with upper magnetic properties by cold sintering process via a non-aqueous solvent," in *Acta Mater.*, vol. 219, p. 117262, 2021. https://doi.org/10.1016/j.actamat.2021.117262.

[7] G. Gultom, M. Rianna, P. Sebayang, and M. Ginting, "The effect of Mg-Al binary doped barium hexaferrite for enhanced microwave absorption performance," *Case Stud. Therm. Eng.*, vol. 18, pp. 0–5, 2020, doi: 10.1016/j.csite.2019.100580.

[8] N. Xia, M. Chen, X. Mao, S. Yan, and H. Ma, "Laminated nanocrystalline-ferrite high saturation magnetic flux density composite core for use in high-frequency transformers," *J. Power Electron.*, no. 0123456789, 2024, doi: 10.1007/s43236-024-00814-4.

[9] M. A. Darwish, A. I. Afifi, A. S. Abd El-Hameed, H. F. Abosheiasha, A. M. A. Henaish, D. Salogub, A. T. Morchenko, V. G. Kostishyn, V. A. Turchenko, and A. V. Trukhanov, "Can hexaferrite composites be used as a new artificial material for antenna applications?," in *Ceram. Int.*, vol. 47, no. 2, pp. 2615–2623, 2021. https://doi.org/10.1016/j.ceramint.2020.09.108

[10] B. C. Manjunatha, P. Puneeth Kumar, N. Pushpa, P. Shankar, and B. M. Nagabhushana, "Study of structural and magnetic features of aluminum substituted hexaferrites of calcium suitable for memory storage application," *Mater. Today Proc.*, vol. 89, no. xxxx, pp. 14–18, 2023, doi: 10.1016/j.matpr.2023.03.637.

[11] F. F. Alharbi, Salma Aman, Naseeb Ahmad, M. A. Almessiere, A. Baykal, and S. A. Al-Heniti, "Eu–Co substituted Sr-hexaferrites for recording media and microwave devices," in *J. Mater. Sci. Mater. Electron.*, vol. 33, no. 15, pp. 12147–12156, 2022. https://doi.org/10.1007/s10854-022-08175-z

[12] S. E. Shirsath, R. H. Kadam, K. M. Batoo, D. Wang, and S. Li, "Co-Al-substituted strontium hexaferrite for rare earth free permanent magnet and microwave absorber application," *J. Phys. D. Appl. Phys.*, vol. 54, no. 2, 2021, doi: 10.1088/1361-6463/abb9d5.

[13] R. Jasrotia, J. Prakash, Himanshi, N. Thakur, K. Raj, A. Kandwal, and P. Sharma, "Advancements in doping strategies for enhancing applications of M-type hexaferrites: A comprehensive review," *Prog. Solid State Chem.*, vol. 72, p. 100427, Dec. 2023. https://doi.org/10.1016/j.progsolidstchem.2023.100427

[14] Y. Marouani, J. Massoudi, M. Noumi, A. Benali, E. Dhahri, P. Sanguino, M. P. F. Graça, M. A. Valente, and B. F. O. Costa, "Electrical conductivity and dielectric properties of Sr doped M-type barium hexaferrite $BaFe_{12}O_{19}$," *RSC Adv.*, vol. 11, no. 3, pp. 1531–1542, Jan. 2021. https://doi.org/10.1039/d0ra09465j

[15] Himanshi, R. Jasrotia, J. Prakash, R. Verma, P. Thakur, A. Kandwal, F. Wan, and A. Thakur, "Synthesis, characterization, and applications of doped barium hexaferrites: A review," *Phys. B Condens. Matter*, vol. 667, p. 415202, Oct. 2023. https://doi.org/10.1016/j.physb.2023.415202

[16] J. Edianta, N. Fauzi, M. Naibaho, F. S. Arsyad, and I. Royani, "Review of the effectiveness of plant media extracts in barium hexaferrite magnets (Bafe12o19)," *Sci. Technol. Indones.*, vol. 6, no. 2, pp. 39–52, 2021, doi: 10.26554/STI.2021.6.2.39-52.

[17] M. Ginting, P. Sebayang, M. Rianna, M. Situmorang, H. Fujiati, A. P. Tetuko, E. A. Setiadi, C. Kurniawan, and A. M. S. Sebayang, "Effect of Co and Ni additions as doping materials on the micro-

structures and the magnetic properties of barium hexa-ferrites," *Case Stud. Therm. Eng.*, vol. 18, p. 100589, 2020. https://doi.org/10.1016/j.csite.2020.100589

[18] S. Chanda, S. Bharadwaj, A. Srinivas, K. V. Siva Kumar, and Y. Kalyana Lakshmi, "Estimation of iron ion distribution at various sites contributing to saturation magnetization in barium hexaferrite at different sintering temperatures," *J. Phys. Chem. Solids*, vol. 155, no. April, 2021, doi: 10.1016/j.jpcs.2021.110120.

[19] T. Charoensuk, W. Thongsamrit, C. Ruttanapun, P. Jantaratana, and C. Sirisathitkul, "Loading effect of sol-gel derived barium hexaferrite on magnetic polymer composites," *Nanomaterials*, vol. 11, no. 3, pp. 1–12, 2021, doi: 10.3390/nano11030558.

[20] V. Turchenko, A. Trukhanov, S. Trukhanov, M. I. Sayyed, M. I. Sayyed, S. Polosan, and A. Trukhanov, "Microscopic mechanism of ferroelectric properties in barium hexaferrites," *J. Alloys Compd.*, vol. 931, p. 167433, 2023. https://doi.org/10.1016/j.jallcom.2022.167433

[21] M. Rianna, M. Situmorang, C. Kurniawan, A. P. Tetuko, E. A. Setiadi, M. Ginting, and S. Simbolon, "The effect of Mg-Al additive composition on microstructure, magnetic properties, and microwave absorption on $BaFe_{12-2x}Mg_xAl_xO_{19}$ (x = 0–0.5) material synthesized from natural iron sand," *Mater. Lett.*, vol. 256, p. 126612, 2019. https://doi.org/10.1016/j.matlet.2019.126612

[22] E. S. Al-Hwaitat, M. K. Dmour, A. S. Masadeh, I. Bsoul, Y. Maswadeh, and S. H. Mahmood, "Effects of pH value and Sintering Temperature on the Structural and Magnetic Properties of Barium Hexaferrites Prepared by Co-Precipitation," *Mater. Sci. Res. India*, vol. 18, no. 1, pp. 37–47, 2021, doi: 10.13005/msri/180105.

[23] M. M. E. Barakat, D. E. S. Bakeer, and A. H. Sakr, "Structural, Magnetic Properties and Electron Paramagnetic Resonance for BaFe12-xHgxO19 Hexaferrite Nanoparticles Prepared by Co-Precipitation Method," *J. Taibah Univ. Sci.*, vol. 14, no. 1, pp. 640–652, 2020, doi: 10.1080/16583655.2020.1761676.

[24] Charishma, V. Veena Devi Shastrimath, R. Bairy, M. S. Murari, A. Jayarama, and R. Pinto, "Structural, morphological and optical properties of barium doped bismuth ferrite thin films deposited by spray pyrolysis," *Mater. Today Proc.*, vol. 35, pp. 440–444, 2019, doi: 10.1016/j.matpr.2020.02.950.

[25] Y. Noratiqah and N. B. Ibrahim, "Pure polycrystalline barium hexaferrite film prepared without buffer layer, using a sol–gel method," *Appl. Phys. A Mater. Sci. Process.*, vol. 129, no. 1, pp. 1–14, 2023, doi: 10.1007/s00339-022-06289-z.

[26] A. Lohmaah, K. Chokprasombat, S. Pinitsoontorn, and C. Sirisathitkul, "Magnetic properties and morphology copper-substituted barium hexaferrites from sol-gel auto-combustion synthesis," *Materials (Basel).*, vol. 14, no. 19, pp. 1–8, 2021, doi: 10.3390/ma14195873.

[27] A. Bhaduri, S. Singh, K. B. Thapa, and B. C. Yadav, "Visible light-induced, highly responsive, below lower explosive limit (LEL) LPG sensor based on hydrothermally synthesized barium hexaferrite nanorods," *Sensors Actuators B Chem.*, vol. 348, no. September, p. 130714, 2021, doi: 10.1016/j.snb.2021.130714.

[28] L. A. Trusov, A. E. Sleptsova, J. Duan, E. A. Gorbachev, E. S. Kozlyakova, E. O. Anokhin, A. A. Eliseev, M. A. Karpov, A. V. Vasiliev, O. A. Brylev, and P. E. Kazin, "Glass-ceramic synthesis of Cr-substituted strontium hexaferrite nanoparticles with enhanced coercivity," *Nanomaterials*, vol. 11, no. 4, p. 924, 2021. https://doi.org/10.3390/nano11040924

[29] G. Muhiuddin, I. Bibi, Z. Nazeer, F. Majid, S. Kamal, A. Kausar, Q. Raza, N. Alwadai, S. Ezzine, and M. Iqbal, "Synthesis of Ni doped barium hexaferrite by microemulsion route to enhance the visible light-driven photocatalytic degradation of crystal violet dye," *Ceram. Int.*, vol. 49, no. 3, pp. 4342–4355, 2023. https://doi.org/10.1016/j.ceramint.2022.09.319

[30] K. Huang, J. Yu, L. Zhang, J. R. Xu, P. Li, Z. Yang, C. Liu, W. Wang, and X. Kan, "Synthesis and characterizations of magnesium and titanium doped M-type barium calcium hexaferrites by a solid state reaction method," *J. Alloys Compd.*, vol. 825, p. 154072, 2020. https://doi.org/10.1016/j.jallcom.2020.154072:contentReference[oaicite:4]{index=4}

[31] P. da Silva-Soares, L. da Costa-Catique, F. Guerrero, P. Mariño-Castellanos, E. Govea-Alcaide, Y. Romaguera-Barcelay, A. R. Rodrigues, E. Padrón-Hernández, and R. Peña-Garcia, "Investigation of structural and magnetic properties of Al substituted $Ba_{0.9}La_{0.1}Fe_{12-x}Al_xO_{19}$ hexaferrites prepared by solid-state reaction method," *J. Magn. Magn. Mater.*, vol. 547, p. 168958, 2022. https://doi.org/10.1016/j.jmmm.2021.168958:contentReference[oaicite:5]{index=5}

[32] A. Kumar, S. Dutta, S. Kim, T. Kwon, S. S. Patil, N. Kumari, S. Jeevanandham, and I. S. Lee,

"Solid-State Reaction Synthesis of Nanoscale Materials: Strategies and Applications," *Chem. Rev.*, vol. 122, no. 15, pp. 12748–12863, 2022. https://doi.org/10.1021/acs.chemrev.1c00637

[33] N. Thakur, I. Sharma, T. Kumari, P. Sharma, and A. Thakur, "Improvement in the structural, magnetic and electromagnetic behaviour of barium hexaferrites with yttrium doping for EMI shielding," *J. Alloys Compd.*, vol. 976, p. 173042, 2024. https://doi.org/10.1016/j.jallcom.2023.173042

[34] Masruroh, A. Manggara, T. Papilaka, and R. T. T, "Penentuan ukuran Kristal (crytallite size) lapisan tipis PZT melalui pendekatan persamaan Debye Scherrer," *Jur. Fis. dan Kim. FMIPA Univ. Brawijaya*, vol. 1, no. 2, pp. 24–29, 2013.